

1 Figures TFIELD-60 and TFIELD-61. Figure TFIELD-60 shows a scatterplot of the modeled
2 steady-state heads in the 121 calibrated T fields versus the measured heads. Also shown is a
3 unit-slope line representing perfect agreement between the measured and modeled heads, and
4 parallel lines showing a 5-m (16-ft) range on either side. Most modeled head values fall within
5 the ± 5 m (16 ft) lines, except for the modeled heads for H-9b, the well with the lowest measured
6 head. As discussed in Section 7.2.1 of this attachment, H-9b is the southernmost well in the
7 model domain and the southern model boundary condition consistently caused the modeled H-9b
8 head to be significantly lower than the measured head.

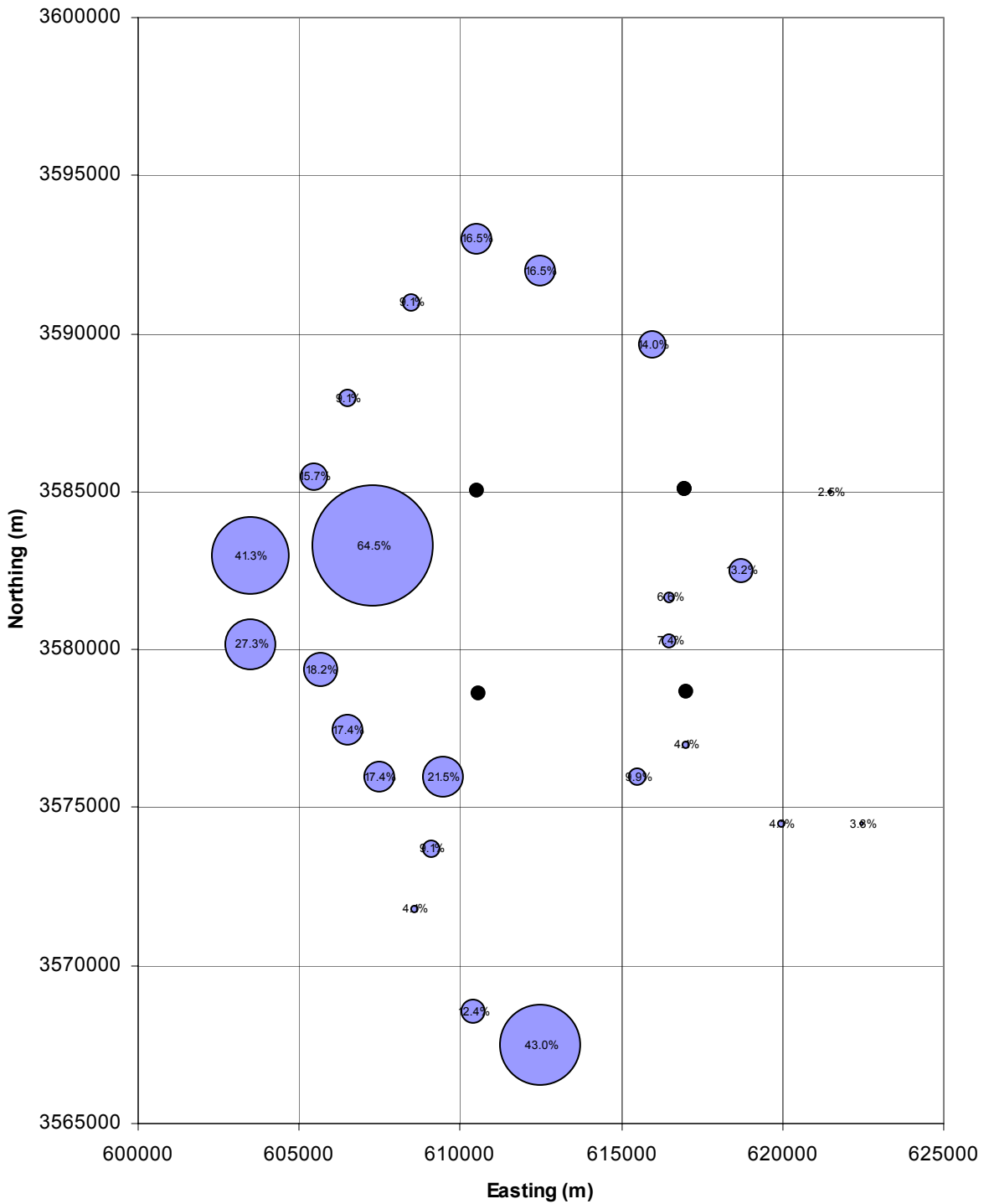
9 Figure TFIELD-61 shows a histogram of the differences between the modeled and measured
10 heads. The majority of modeled head values more than 8 m (26 ft) lower than the measured
11 values are associated with H-9b. Excluding the H-9b values, the histogram shows a normal
12 distribution of errors with 48 percent of the modeled heads within 2 m (7 ft) of the measured
13 heads, and 79 percent of the modeled heads within 4 m (13 ft) of the measured heads. The fit
14 between measured and modeled steady-state heads could probably have been improved by
15 allowing PEST to perform more calibration iterations but, as shown in Section 7.3 of this
16 attachment, the travel-time distribution for the T fields would be unlikely to be affected.

17 ***TFIELD-8.3 Pilot-Point Sensitivity***

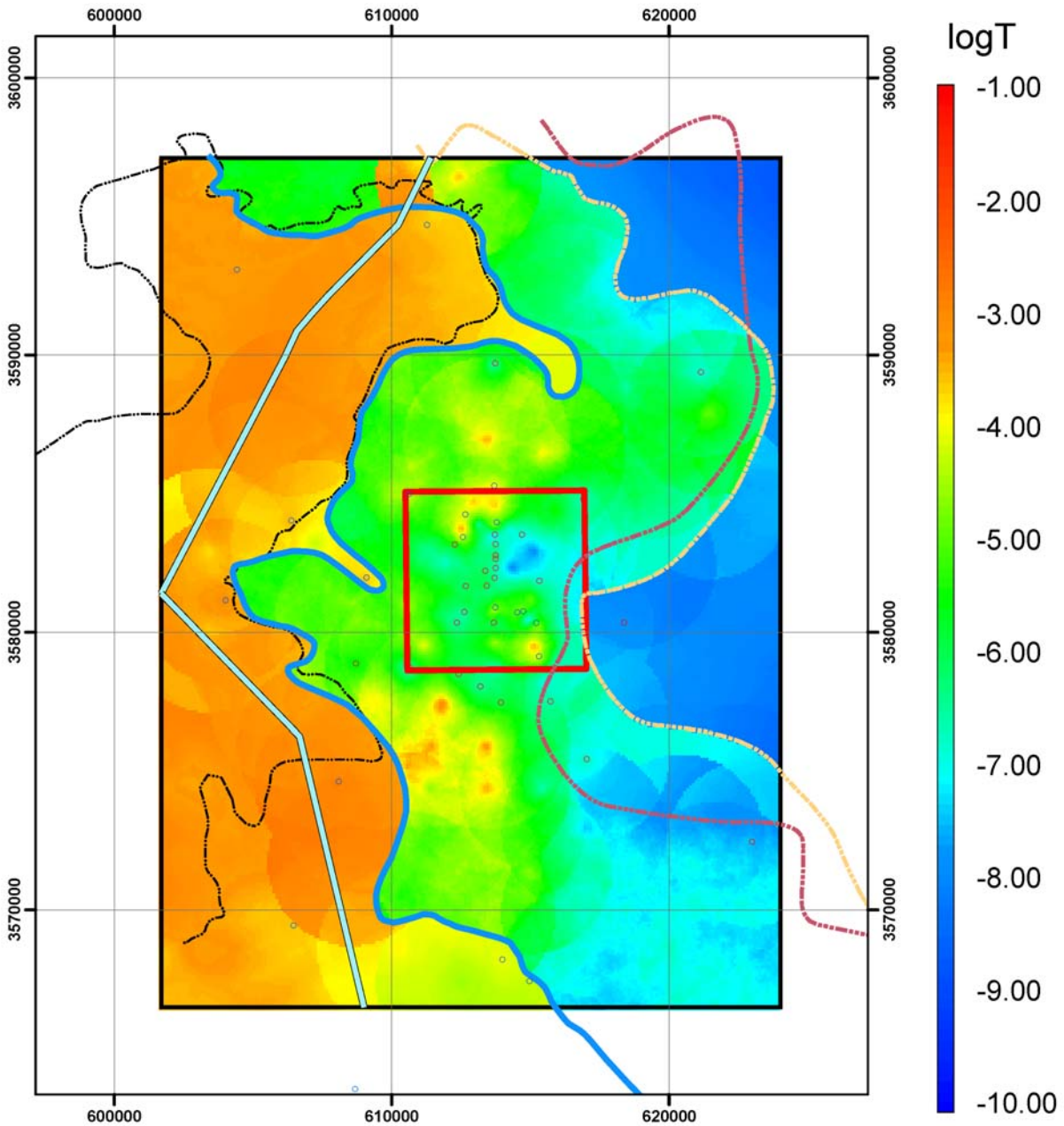
18 Transmissivities at each of the pilot points within the model domain were altered during the
19 calibration process. The maximum allowable change was \pm three orders of magnitude in the
20 middle region of the model domain and \pm one order of magnitude in the low-T (eastern) and
21 high-T (western) regions of the model domain. Figures TFIELD-62 and TFIELD-63 show the
22 percentage of calibrated T fields in which each pilot point hit the maximum and minimum
23 possible value, respectively. The size of the bubble is proportional to the number of times the
24 value hits one constraint or the other. Figure TFIELD-62 shows that the pilot points south of the
25 western portion of the southern LWB were most likely to reach their maximum allowable values,
26 indicating that the base T fields may have underestimated Ts in this area. Figure TFIELD-63
27 shows that the pilot point placed in the inferred dissolution reentrant between P-14 and WIPP-25
28 west of the LWB (see Figure TFIELD-38) was most likely to reach its minimum allowable
29 value, indicating that this reentrant may not be as hydraulically significant as originally assumed.

30 ***TFIELD-8.4 Ensemble Average T Field***

31 The 121 T fields that were acceptably calibrated can be combined into an ensemble average T
32 field showing the average properties of the T fields (Figure TFIELD-64). The averaging is
33 performed on a cell-by-cell basis, taking the arithmetic mean of the 121 T values assigned to
34 each cell. Figure TFIELD-65 shows a close-up view of the ensemble average of the 100 T fields
35 used for subsequent calculations in the area surrounding the WIPP site, using a different color
36 scale with T values “binned” by order of magnitude for clarity. This figure does not show a
37 continuous north-south high-T zone exiting the southeastern portion of the WIPP site, as was
38 present in the ensemble average T field provided in CCA Appendix TFIELD (Figure 30). It also
39 shows higher Ts in the southwestern portion of the WIPP site than were present in the CCA
40 ensemble average field. These differences explain why the travel paths in the CRA-2004 T
41 fields (Figure TFIELD-58) take a more westerly course, on average, than those in the CCA T



1
 2 **Figure TFIELD-61. Percentage of T Fields in which Pilot Points Hit Minimum Allowable**
 3 **Values. Corners of WIPP LWB are shown by unlabeled black dots.**
 4



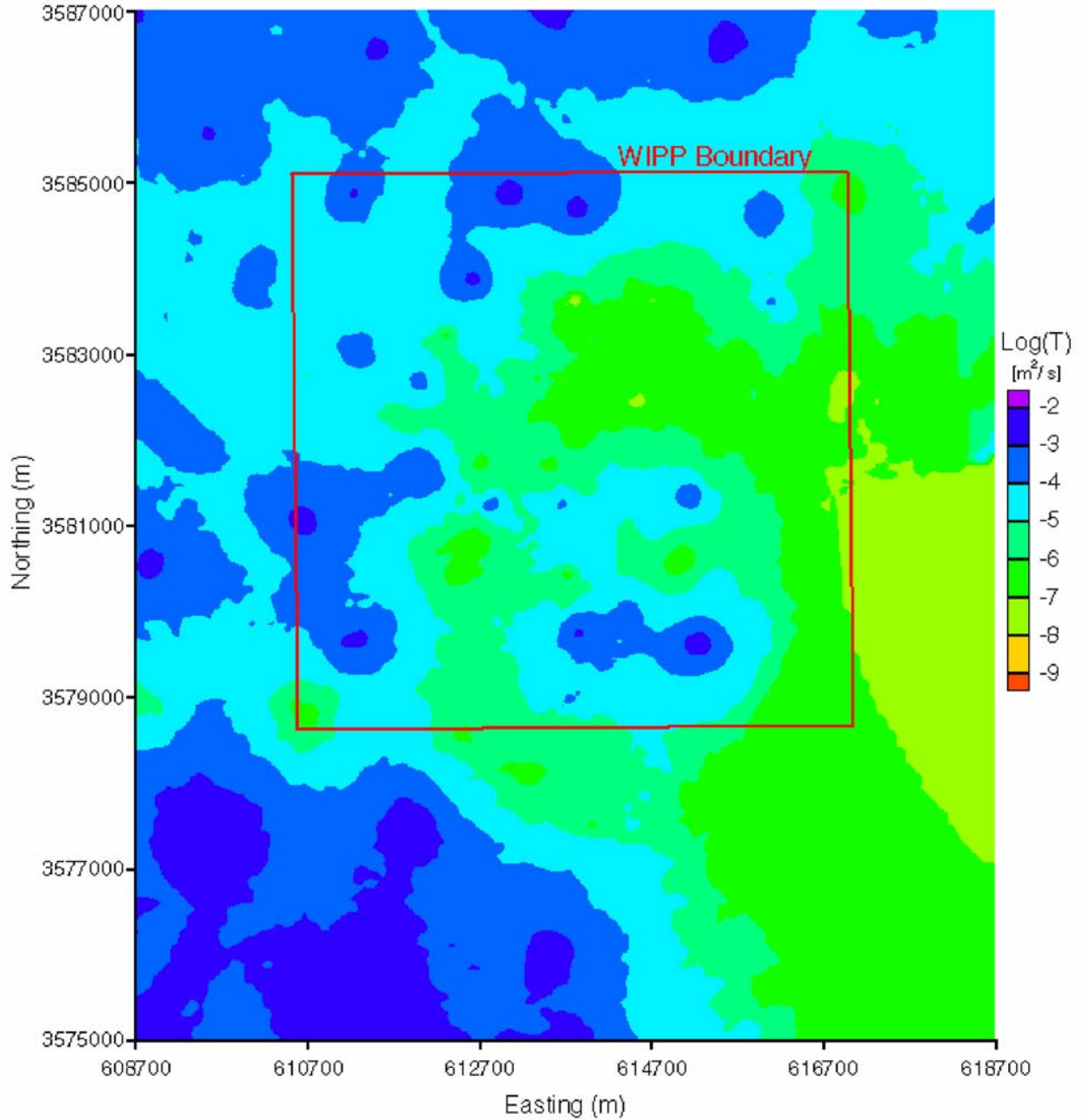
Explanation

- | | |
|------------------------------|--|
| Well (transmissivity) | ----- Nash Draw |
| • Low | — Salado Dissolution |
| • High | WIPP Site |
| ----- Salt Margin m3/h3 | — No Flow Boundary |
| ----- Salt Margin m2/h2 | |



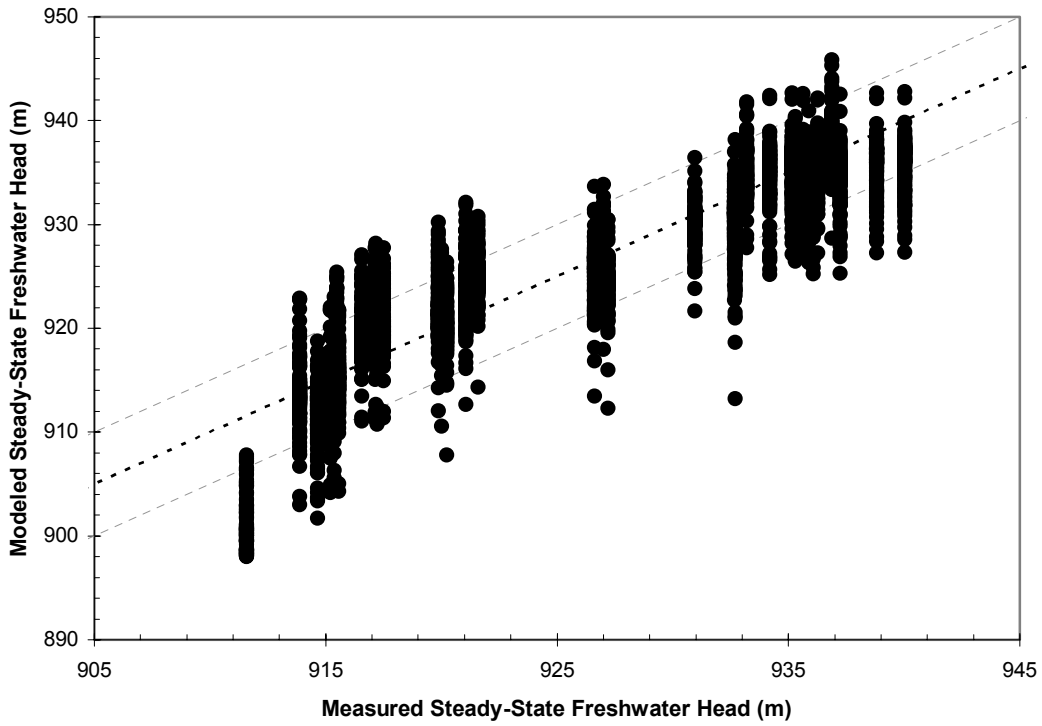
1
2

Figure TFIELD-62. Ensemble Average of 121 Calibrated T Fields



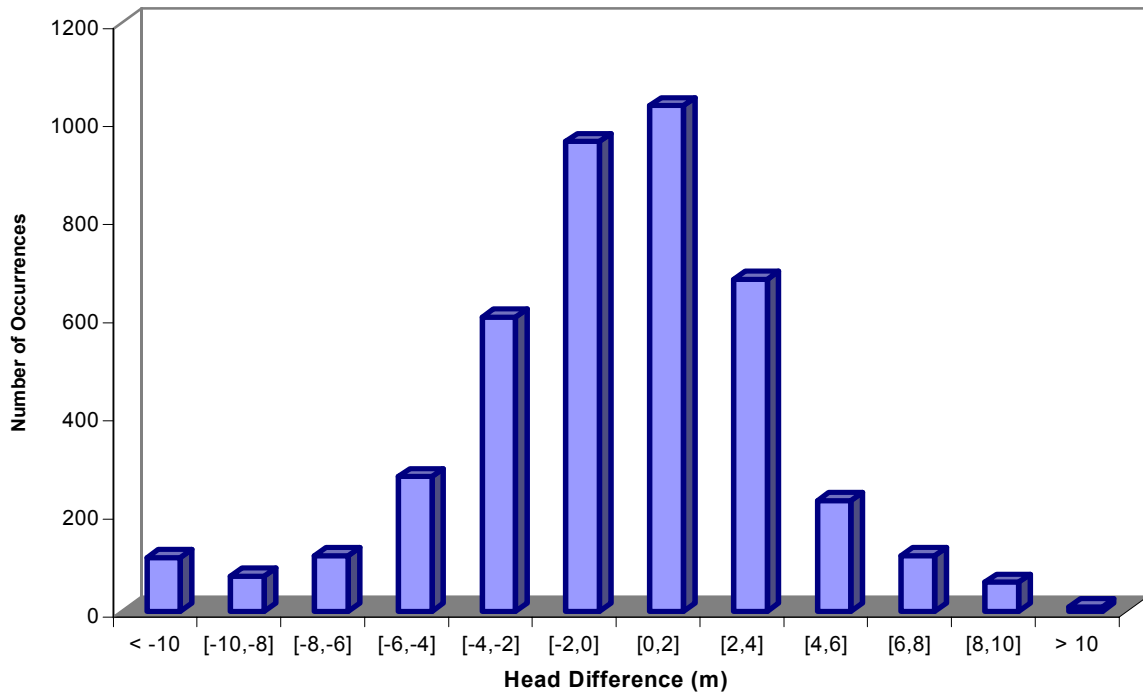
1

2 **Figure TFIELD-63. Close-Up View of the Ensemble Average T Field Near the WIPP Site.**
3 **Note the different log₁₀ color scale from Figure TFIELD-62.**



1
2
3

Figure TFIELD-64. Scatterplot of Measured Versus Modeled Steady-State Heads



4
5
6

Figure TFIELD-65. Histogram of Differences Between Measured and Modeled Steady-State Heads

1 fields, and why the CRA-2004 travel times are longer than the CCA travel times (Figure
2 TFIELD-57).

3 ***TFIELD-9.0 MODIFICATION OF T FIELDS FOR MINING SCENARIOS***

4 The WIPP site lies within the Carlsbad mining district of southeastern New Mexico. Potash mining
5 in the WIPP area involves resource extraction below the Culebra in the underlying McNutt potash
6 zone of the Salado. In the future, potash mining is expected to occur in all areas where
7 economically extractable ore is present, both outside and inside the WIPP LWB. It is hypothesized
8 that mining of potash leads to subsidence and fracturing of the Culebra, resulting in increased
9 Culebra T. This increase in T may change the regional groundwater flow pattern in the Culebra
10 and affect the transport of any radionuclides entering the Culebra from the WIPP repository.

11 The EPA (1996, p. 5242) guidance for how the potential effects of future mining should be
12 considered in WIPP PA follows:

13 40 CFR §194.32, Scope of performance assessments.

- 14 (a) Performance assessments shall consider natural processes and events, mining, deep drilling,
15 and shallow drilling that may affect the disposal system during the regulatory time frame.
- 16 (b) Assessments of mining effects may be limited to changes in the hydraulic conductivity of the
17 hydrogeologic units of the disposal system from excavation mining for natural resources.
18 Mining shall be assumed to occur with a one in 100 probability in each century of the
19 regulatory time frame. Performance assessments shall assume that mineral deposits of those
20 resources, similar in quality and type to those resources currently extracted from the Delaware
21 Basin, will be completely removed from the controlled area during the century in which
22 such mining is randomly calculated to occur. Complete removal of such mineral resources
23 shall be assumed to occur only once during the regulatory time frame.
- 24 (c) Performance assessments shall include an analysis of the effects on the disposal system of any
25 activities that occur in the vicinity of the disposal system prior to disposal and are expected to
26 occur in the vicinity of the disposal system soon after disposal. Such activities shall include,
27 but shall not be limited to, existing boreholes and the development of any existing leases that
28 can reasonably be expected to be developed in the near future, including boreholes and leases
29 that may be used for fluid injection activities.

30 The EPA (1996, p. 5229) further states:

31 In order to consider the effects of mining in performance assessments, DOE may use the location-
32 specific values of hydraulic conductivity, established for the different spatial locations within the
33 Culebra dolomite, and treat them as sampled parameters with each having a range of values
34 varying between unchanged and increased 1,000-fold relative to the value that would exist in the
35 absence of mining.

36 Accordingly, for PA purposes, the DOE assumes that all economically extractable potash is
37 mined outside of the WIPP LWB during the 100 years after closure of the WIPP repository
38 during which active institutional control of the site is maintained. Following that 100-year
39 period, the DOE assumes there is a one in 100 probability that the potash within the LWB will be
40 mined during any given century. Therefore, all PA calculations of transport of radionuclides
41 released to the Culebra through inadvertent human intrusion of the repository assume that all
42 potash outside the LWB has already been mined (the “partial-mining” scenario) by the time the

1 intrusion occurs. The “full-mining” scenario is invoked when the sampled time of human
2 intrusion is coincident with or later than the sampled time of mining within the LWB. Under
3 both scenarios, the hydraulic conductivity (or T) of the Culebra is assumed to be increased by a
4 random factor between one and 1,000 in the areas affected by mining. The process by which the
5 calibrated Culebra T fields were modified to account for the effects of mining, and the
6 characteristics of the resulting modified T fields, are discussed below.

7 ***TFIELD-9.1 Determination of Potential Mining Areas***

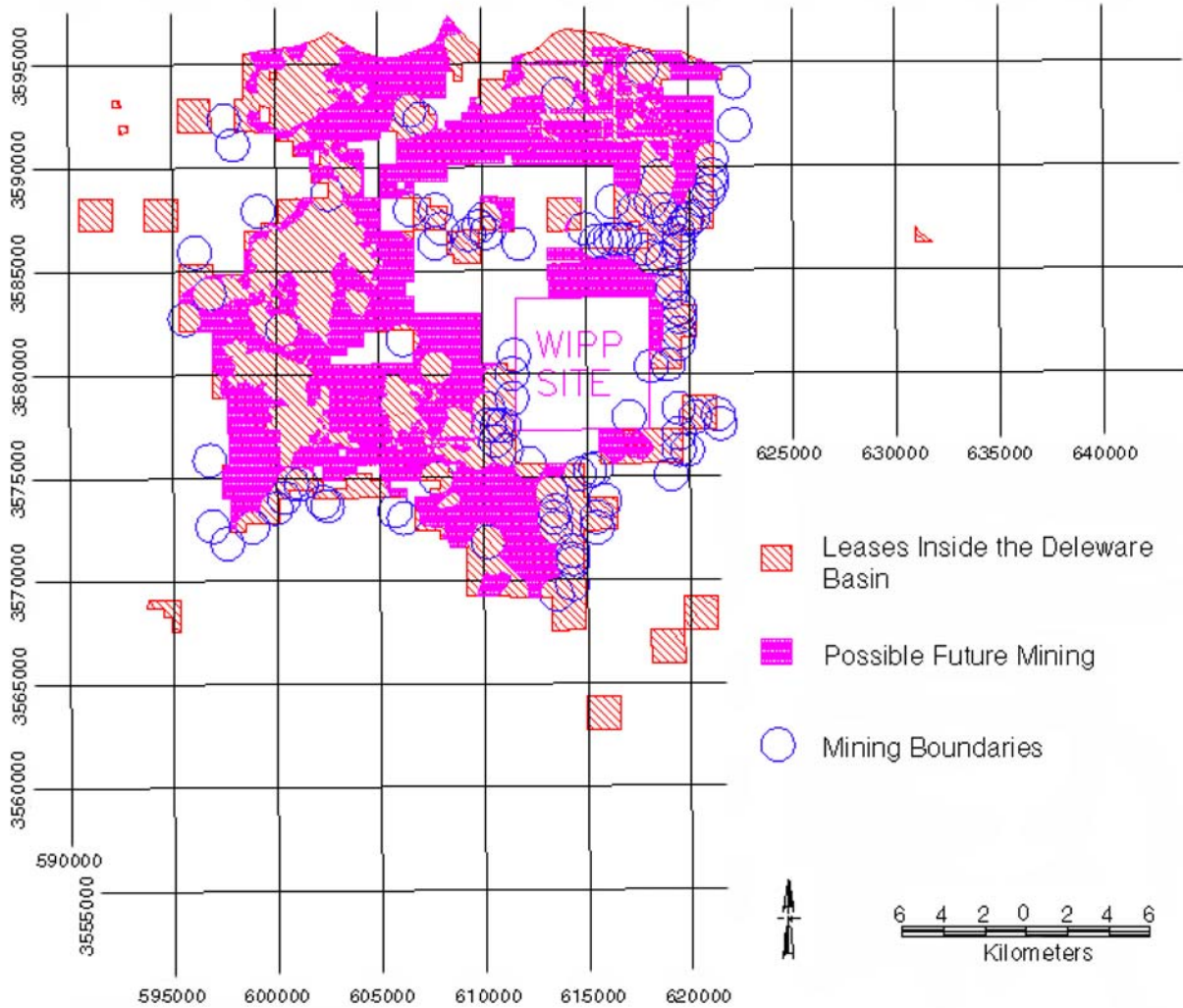
8 Figure TFIELD-66 shows current potash mines and economically recoverable resources (reserves)
9 in the known potash lease area around the WIPP site, which are the areas where subsidence
10 might occur in the future. The map is based on the BLM (1993) map “Preliminary Map Showing
11 Distribution of Potash Resources, Carlsbad Mining District, Eddy and Lea Counties, New
12 Mexico.” Whereas the BLM map shows all reserves, Figure TFIELD-66 shows only reserves
13 that are within existing leases and that are outside the one-quarter to one-half mile (402 to 805
14 m) exclusion zones around oil and gas wells. Potash reserves outside the current leases will most
15 likely never be mined because active oil and gas exploration is now underway in those areas.

16 This map is periodically updated as part of the Delaware Basin Drilling Surveillance Program. It
17 also shows the locations of petroleum industry boreholes in the vicinity. The current version of
18 the map differs from the one used for the CCA calculations in that several areas north of the
19 LWB have been ruled out as potential mining areas in the updated version due to recent oil and
20 gas drilling in those areas. Figure TFIELD-67 shows the estimated extent of economically
21 extractable potash within the WIPP LWB.

22 Because the potash mining horizon is located in the Salado Formation, below the Culebra, the
23 areas in the Culebra that might be disturbed by the mining activities are larger than shown on
24 Figures TFIELD-66 and TFIELD-67 due to angle-of-draw effects associated with subsidence.
25 The rationale for determining the extent of these effects is described in Wallace (1996) with the
26 final conclusion stating that an additional 253-m (830-ft)-wide “collar” was to be added to the
27 mining-impacted areas to approximate a 45-degree angle of draw. For the current T fields, a
28 buffer of three cell widths (300 m [984 ft]) was manually digitized and added to the mining
29 zones. This new delineation was then compared to the CCA model mining zones to make sure
30 there were no significant differences outside of those that can be explained by different gridding
31 of the two model domains and the addition of new data (Figure TFIELD-68). The most notable
32 difference between the two versions is that the area of potential future mining along the
33 northeastern boundary of the LWB is no longer directly connected to the northern boundary of
34 the model domain, which would be expected to decrease flow to the WIPP site.

35 ***TFIELD-9.2 Scaling of Transmissivity***

36 For each of the final 100 T fields selected as described in Section 7.4 of this attachment, a
37 random transmissivity multiplier between 1 and 1,000 was assigned using Latin hypercube
38 sampling (LHS) (***Long 2004***). That multiplier was then applied to the modeled T values in the
39 mining-affected areas shown in Figure TFIELD-68 outside of the WIPP LWB to create a partial-
40 mining T field, and to the modeled T values in mining-affected areas both inside and outside the
41 LWB to create a full-mining T field. LHS was performed three times to provide three replicates
42 of 100 full-mining and 100 partial-mining T fields. The purpose of using three replicates is to

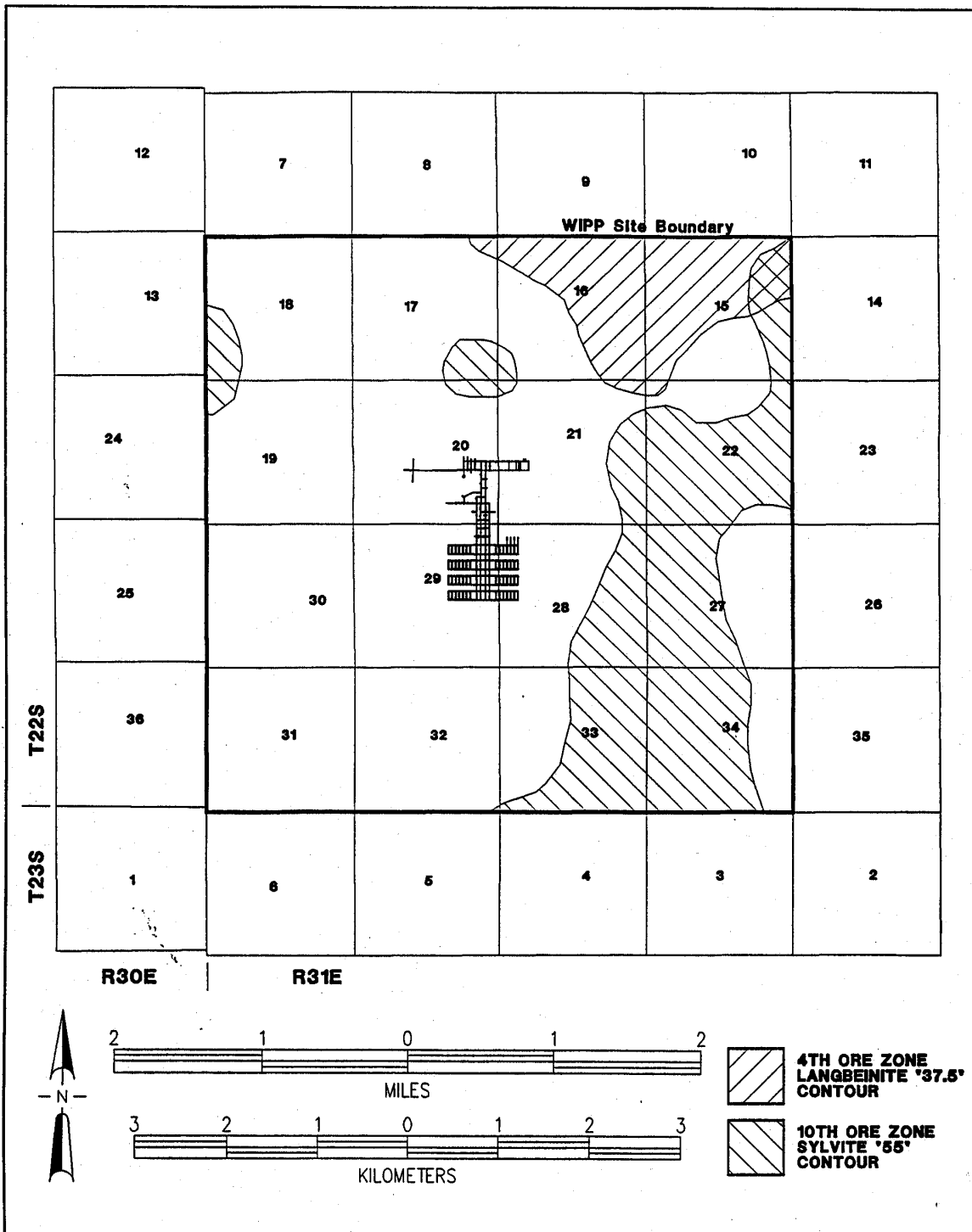


1
2 **Figure TFIELD-66. Leased Potash Resources Near the WIPP Site**

3 demonstrate that the LHS has adequately captured the uncertainty in the T fields. The
4 transmissivity multipliers applied to each field for the three replicates are shown in Table
5 TFIELD-12.

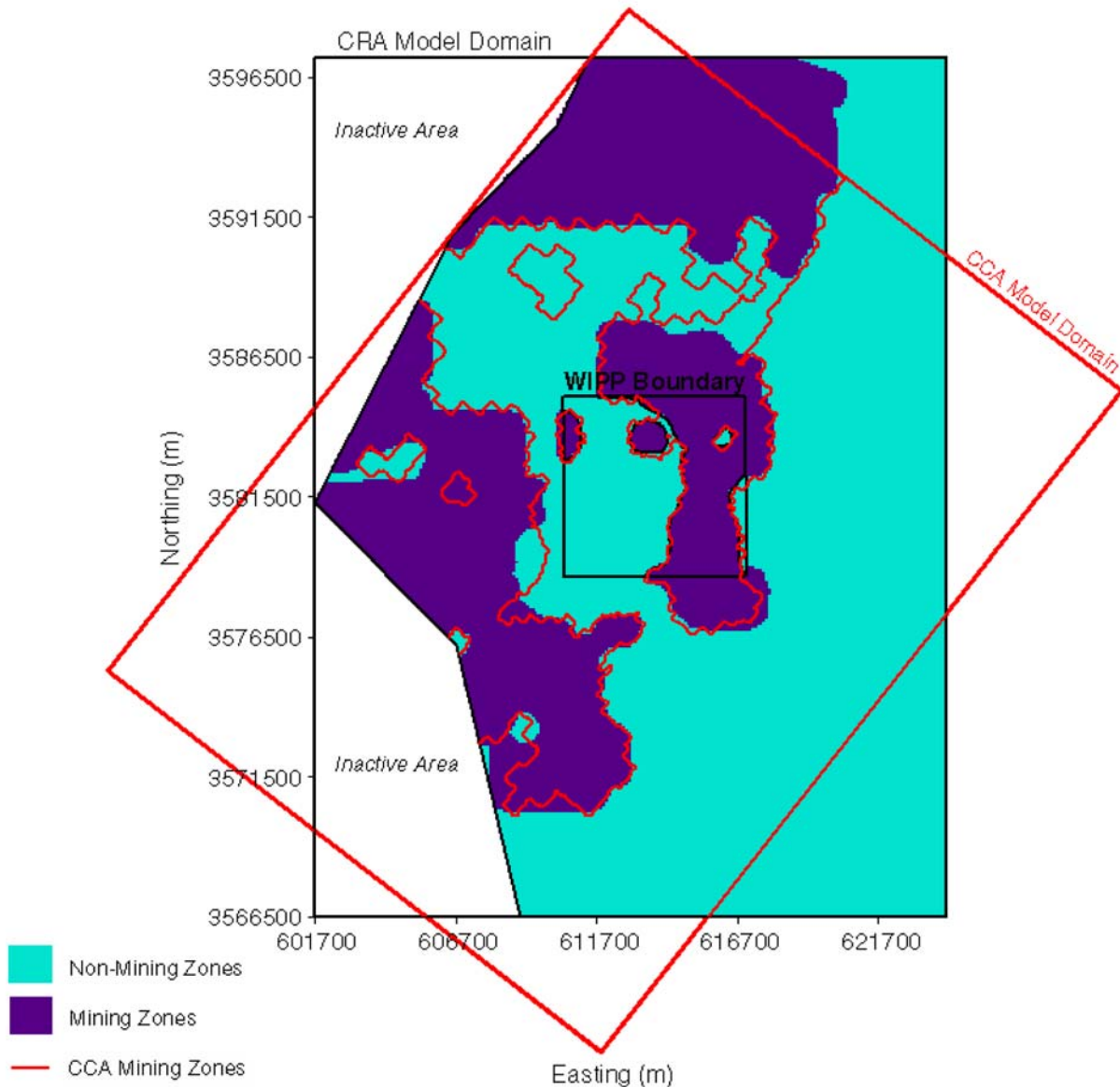
6 **TFIELD-9.3 Forward Runs**

7 A forward steady-state flow model was run for each of the 100 new T fields under each mining
8 scenario (full and partial) for the three replicates of transmissivity multipliers, resulting in 600
9 simulations. Particle tracking was performed using DTRKMF on the modified flow fields to
10 determine the flow path and groundwater travel time from a point above the center of the WIPP
11 disposal panels to the LWB. A CDF was produced for each mining scenario (as well as an
12 undisturbed scenario) that describes the probability of a conservative tracer reaching the LWB at
13 a given time.



1

2 **Figure TFIELD-67. Potential Potash Distribution Within the WIPP LWB. The repository**
 3 **excavations are shown in the center.**



1
2 **Figure TFIELD-68. Comparison of CRA-2004 and CCA Areas Affected by Mining**

3 As was done for the CCA, it was assumed that mining impacts would not significantly change
4 the boundary conditions used in T-field calibration. Potash mining has already occurred along
5 the northern boundary of the model domain, and the western model boundary is in Nash Draw
6 where subsidence and fracturing of the Culebra are already incorporated in the model.

7 ***TFIELD-9.4 Results***

8 ***TFIELD-9.4.1 Travel Times***

9 Figure TFIELD-69 shows CDFs of travel time for the unmodified T fields and for the
10 Replicate 1 full- and partial-mining T fields. The partial-mining travel times are consistently
11 longer than the no-mining travel times. The distribution of travel times for the full-mining case

Table TFIELD-12. T-Field Transmissivity Multipliers for Mining Scenarios

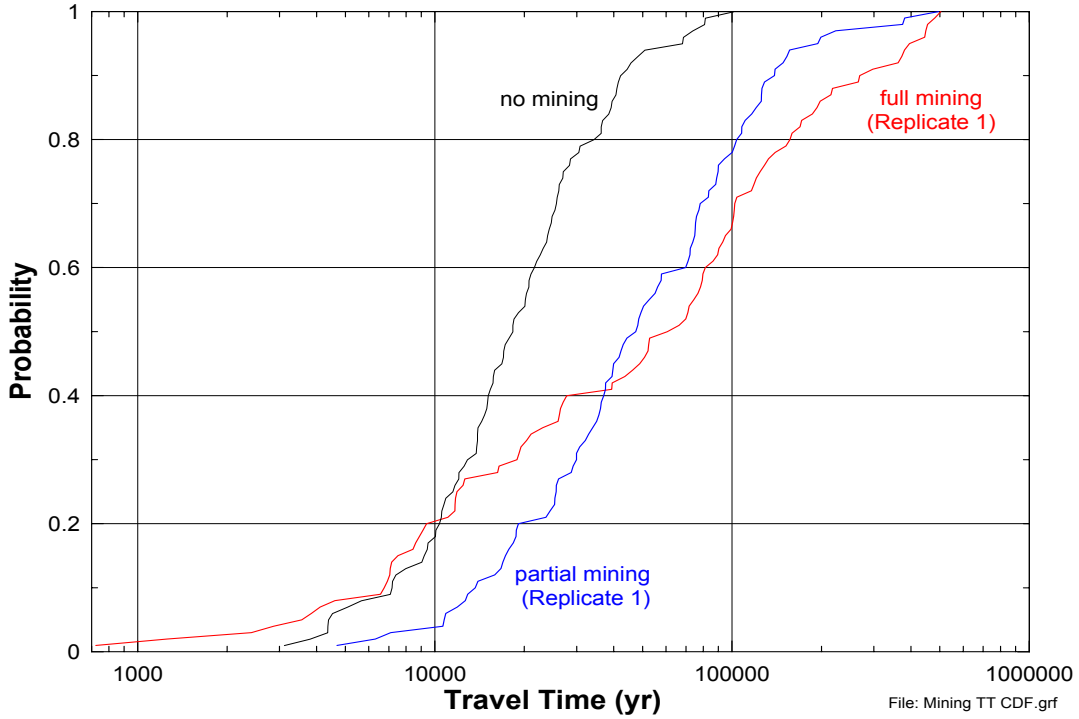
T Field	Replicate 1 Multiplier	Replicate 2 Multiplier	Replicate 3 Multiplier	T Field	Replicate 1 Multiplier	Replicate 2 Multiplier	Replicate 3 Multiplier
d01r02	905.50	32.85	13.54	d09r08	66.07	339.80	327.30
d01r04	508.40	345.10	202.20	d09r09	375.70	806.30	374.20
d01r07	340.30	996.50	936.30	d09r10	521.10	906.90	24.83
d01r10	615.20	828.20	391.80	d10r02	181.60	274.60	651.90
d02r02	575.30	579.30	306.80	d10r03	298.50	796.60	816.70
d03r01	104.00	760.50	955.80	d10r04	705.30	364.70	518.20
d03r03	94.06	514.90	77.79	d10r06	84.20	819.40	690.80
d03r06	913.30	187.60	238.40	d10r07	627.30	728.60	551.20
d03r07	630.50	567.10	725.20	d10r08	403.20	414.80	670.30
d03r08	208.90	475.90	85.67	d10r09	464.20	649.90	885.40
d03r09	769.30	750.00	647.80	d10r10	821.40	607.80	925.70
d04r01	130.20	630.30	478.70	d11r01	307.60	895.10	492.90
d04r02	351.90	453.30	996.70	d11r02	236.50	918.30	364.50
d04r03	46.87	310.90	123.90	d11r06	249.90	159.70	5.43
d04r04	194.60	487.90	217.30	d11r07	543.50	86.78	966.70
d04r05	806.90	923.80	138.30	d11r08	18.75	16.92	973.80
d04r06	264.40	584.00	835.30	d11r09	215.40	618.30	576.30
d04r07	931.50	733.90	802.00	d11r10	73.60	168.90	403.20
d04r08	897.90	51.08	96.80	d12r01	317.40	683.30	756.20
d04r10	32.56	256.50	34.02	d12r02	958.60	204.90	598.10
d05r03	394.10	108.30	159.00	d12r03	686.00	322.00	333.80
d05r07	998.20	535.90	145.50	d12r05	860.70	637.50	589.70
d06r02	790.00	679.40	826.70	d12r06	363.80	359.00	56.05
d06r03	384.10	171.20	261.20	d12r07	660.40	434.90	463.10
d06r04	258.50	860.00	293.90	d12r08	940.20	708.20	312.10
d06r05	432.50	754.10	257.60	d12r09	132.50	464.10	794.60
d06r06	10.02	653.20	172.50	d13r01	983.00	971.30	901.70
d06r07	514.10	221.50	915.60	d13r02	672.80	144.50	224.80
d06r10	282.90	70.11	861.40	d13r03	643.20	849.00	415.20
d07r01	927.30	694.20	625.20	d13r05	425.80	118.60	688.00
d07r02	691.30	864.90	737.80	d13r06	961.10	785.90	385.40
d07r05	738.40	775.30	241.60	d13r07	346.10	282.90	711.40
d07r06	450.20	591.70	548.70	d13r08	838.60	78.26	64.98
d07r07	609.60	447.20	841.00	d13r09	491.00	8.68	458.00
d07r08	557.70	942.30	349.00	d21r01	755.40	307.30	632.40
d07r09	538.60	98.94	285.00	d21r02	172.60	396.20	614.80
d07r10	713.60	379.60	187.30	d21r03	591.50	422.30	45.61

**Table TFIELD-12. T-Field Transmissivity Multipliers for Mining Scenarios
(Continued)**

T Field	Replicate 1 Multiplier	Replicate 2 Multiplier	Replicate 3 Multiplier	T Field	Replicate 1 Multiplier	Replicate 2 Multiplier	Replicate 3 Multiplier
d08r01	849.30	408.40	194.00	d21r04	322.70	715.50	276.80
d08r02	569.70	989.10	893.90	d21r05	855.70	870.90	105.80
d08r03	419.50	43.16	356.30	d21r06	272.00	501.20	984.40
d08r04	160.00	834.00	857.00	d21r07	652.50	296.70	940.20
d08r05	971.90	881.10	671.60	d21r10	790.50	212.70	562.50
d08r06	118.80	558.90	743.20	d22r02	163.20	527.50	870.60
d08r07	741.30	130.20	706.70	d22r03	812.70	264.30	534.50
d09r02	729.70	497.00	429.30	d22r04	144.70	140.70	526.30
d09r03	483.00	197.30	168.20	d22r06	26.04	962.70	111.70
d09r04	580.60	661.30	766.40	d22r07	870.30	548.10	609.10
d09r05	228.50	240.90	481.90	d22r08	773.60	235.30	771.70
d09r06	474.10	383.50	449.10	d22r09	53.04	937.70	784.10
d09r07	887.20	952.10	503.30	d22r10	460.40	24.35	434.60

1 is much wider than for the other two cases; some of the full-mining travel times are shorter than
 2 the no-mining times, but most are considerably longer. The median travel times across all three
 3 replicates for the full- and partial-mining scenarios are approximately 3.6 and 2.6 times greater,
 4 respectively, than for the non-mining scenario. Figures TFIELD-70 and TFIELD-71 compare
 5 the CDFs of travel time for all three replicates of the partial- and full-mining cases, respectively,
 6 to the Replicate 1 results from the CCA T fields (Wallace 1996). These plots show, first, that all
 7 three CRA-2004 replicates provided very similar results and, second, that the new travel times
 8 are consistently longer than the CCA travel times. The primary reason for this difference is
 9 probably the absence in the CRA-2004 T fields of the direct, high-T connection between the
 10 WIPP site and the northern model boundary that was present in the CCA T fields and that
 11 provided a source of water to the Culebra within the LWB. As discussed in Section 9.1 of this
 12 attachment, this difference occurs because recent oil and gas exploratory drilling has precluded
 13 potash mining a few kilometers northeast of the LWB (see Figure TFIELD-66).

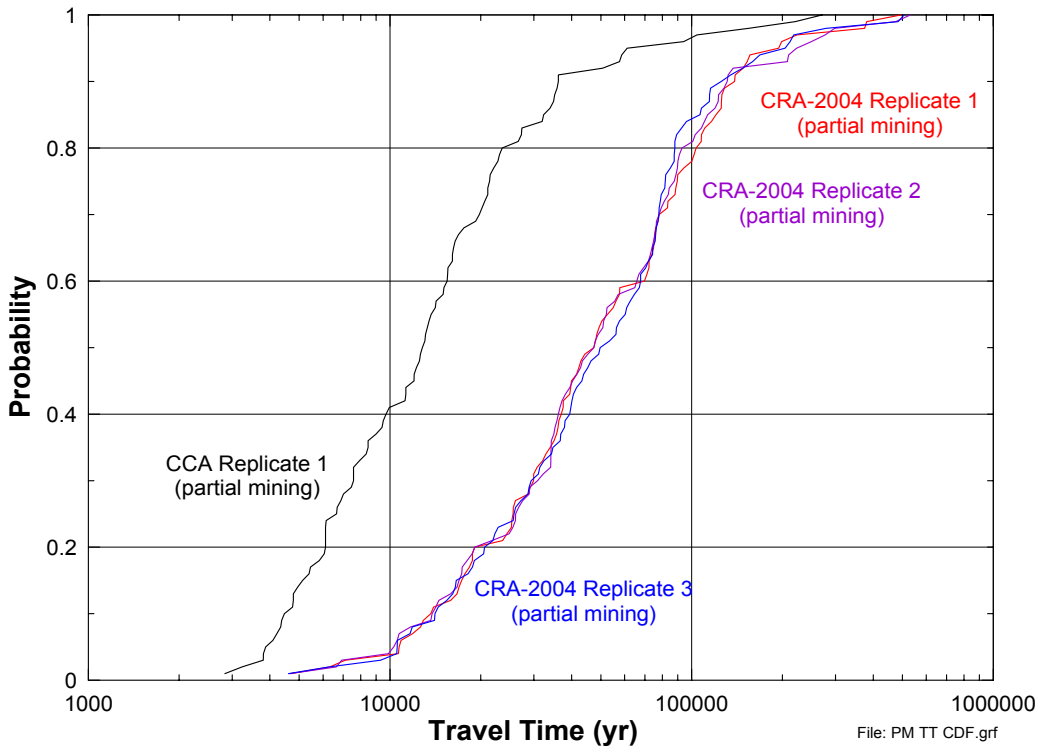
14 Given the increase in transmissivity due to mining, the increase in travel time may seem counter-
 15 intuitive. However, upon examination of the head contours and flow patterns of the mining
 16 cases, the high-T areas corresponding to the mining zones create preferential pathways through
 17 the system. Figure TFIELD-72 shows the normalized velocity in each cell for the
 18 T field/replicate averaged case for the full-mining scenario. The normalized velocity is the
 19 velocity magnitude in each cell divided by the maximum velocity magnitude across the domain.
 20 Since the velocity magnitudes are highly skewed, the color bands for Figure TFIELD-72 are
 21 nonuniformly scaled at the high end (i.e., a wider range of velocity magnitudes is used to
 22 designate the orange and red bands). This allows for a better qualitative comparison of the
 23 spatial distribution of high and low velocities. “T field/replicate averaged” means the T value for



1

2

Figure TFIELD-69. CDFs of Travel Times for the Full-, Partial-, and No-Mining Scenarios

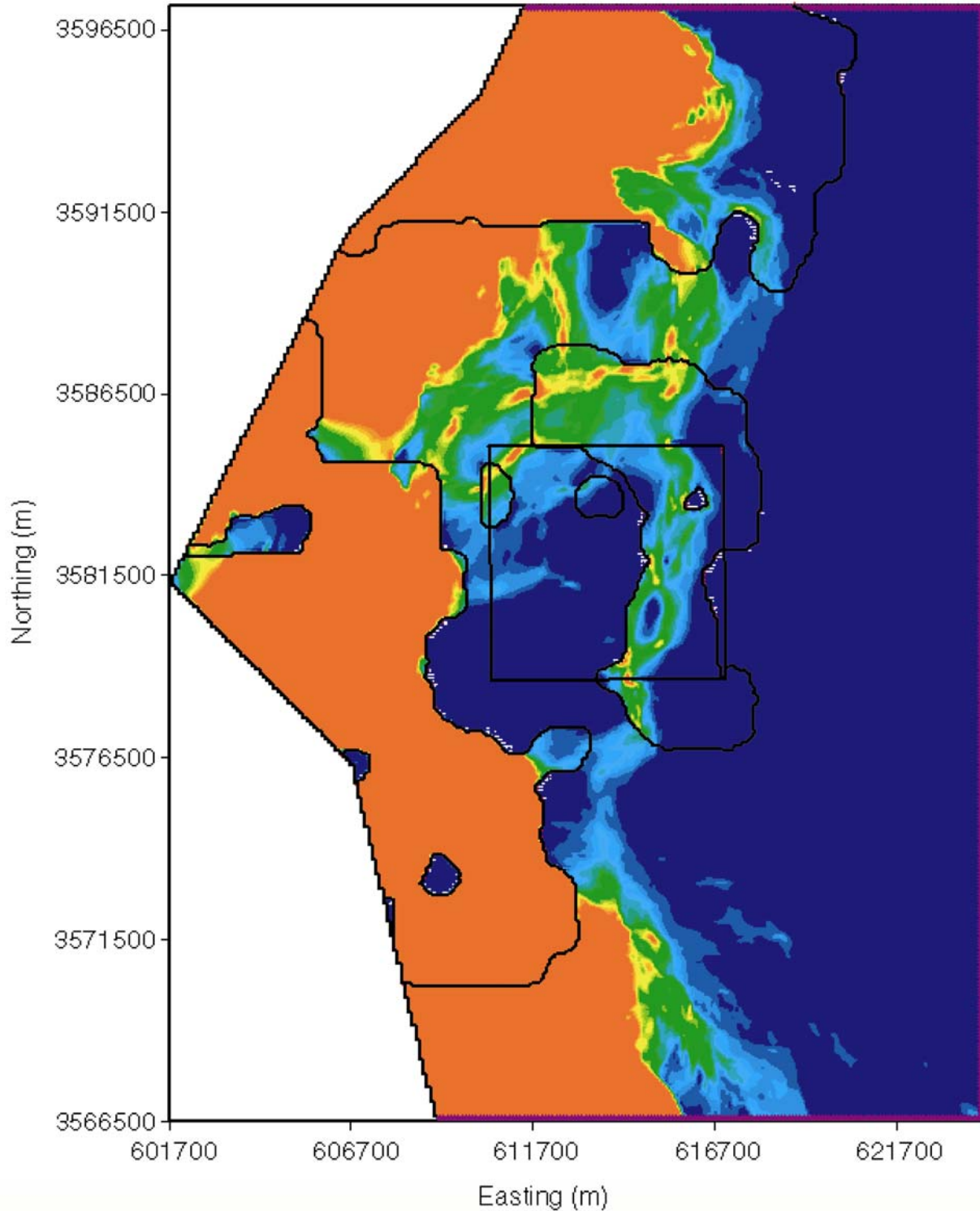


3

4

5

Figure TFIELD-70. CDFs of Partial-Mining Travel Times for Three CRA-2004 Replicates and One CCA Replicate



1
2 **Figure TFIELD-71. Normalized Pore Velocities for the Full-Mining Case. Red indicates**
3 **zones of high velocity. The black outline shows the full-mining zones and the red box is the**
4 **WIPP LWB. The T field used to produce the velocity profile is averaged across all T**
5 **field/replicate combinations for the full-mining scenario (300 T fields in total).**
6